Theoretical Spectroscopy of Inner-Shell Electronic Processes and Photochemistry of Fluorescent Molecules

Masahiro Ehara and Hiroshi Nakatsuji

Abstract The SAC-CI method has been applied to the theoretical spectroscopy of the inner-shell electronic processes and the photochemistry of the organic light-emitting diodes (OLED) and biological chemosensors. Wide varieties of the core-electronic processes such as core-electron ionizations, shake-up satellites, vibrational excitations, valence–Rydberg coupling, and its thermal effect have been investigated by the SAC-CI calculations. The method has also been applied to the electronic spectra and the excited-state dynamics of the polymer materials of OLED such as poly *para*-phenylene vinylene and fluorene-thiophene. The photochemistry of the biological chemosensor has been elucidated in particular for the photo-induced electron transfer mechanism of the acridine-type fluorescent probe.

Keywords: SAC-IC · Theoretical spectroscopy · Inner-cell electronic processes · Organic-light emitting diodes · Priological chemosensors

1 Introduction

Recently, investigations of the core-electronic processes invoked renewal of interest, because significant developments in both high-resolution soft X-ray spectroscopy and accurate state-of-the-art theoretical methods have made us possible to obtain precise knowledge of the core-electronic processes. One can observe vibrational structures in the core-level photoelectron spectrum and thereby discuss the excited-state dynamics. This situation has motivated intensive cooperative researches on the core-electron processes from the experimental and theoretical sides.

Masahiro Ehara (✉)
Institute for Molecular Science, 38 Nishigo-Naka, Myodaiji, Okazaki 444-8585, Japan; JST, CREST, Sanboncho-5, Chiyoda-ku, Tokyo 102-0075, Japan, e-mail: ehara@ims.ac.jp

Hiroshi Nakatsuji
Quantum Chemistry Research Institute, Kyodai Katsura Venture Plaza 106, Kyoto 615-8245, Japan; JST, CREST, Sanboncho-5, Chiyoda-ku, Tokyo 102-0075, Japan,
e-mail: h.nakatsuji@qcri.or.jp

P. Piecuch et al. (eds.), *Advances in the Theory of Atomic and Molecular Systems*, Progress in Theoretical Chemistry and Physics 20, DOI 10.1007/978-90-481-2985-0_6,

The photochemistry of fluorescent molecules like organic light-emitting diodes (OLED) and biological chemosensors is an attractive and important subject. The OLED is recognized as one of the promising candidates for the next generation electro-optical devices. Theoretical interpretation and prediction of the photophysical properties of the OLED molecules are relevant for developing the new materials. The fluorescent probe which works as biological chemosensor has also been focused and extensively investigated, since it enables the direct and real-time measurements of the enzyme activities. The fluorescence change by the interaction with the enzyme is essential and the elucidation of the electronic mechanism of the fluorescence and the color-tuning are important for developing new fluorescent probes.

In the series of our recent works, we have investigated the theoretical spectroscopy of the inner-shell electronic processes and the photochemistry of organic light-emitting diodes and biological chemosensors with the SAC-CI method. The SAC-CI method [1–3] has been successfully applied to the wide varieties of chemistry in particular for the molecular excited states. The method has been established as an accurate molecular excited-state theory applicable to the various kinds of electronic processes in the wide energy region [3–5]. In this chapter, we review our recent SAC-CI studies on the inner-shell electronic processes [6–18] and the organic light-emitting diodes [19, 20] and biological chemosensors.

2 Theoretical Spectroscopy of Inner-Shell Electronic Processes

Core-electron ionization spectra contain the information not only about inner-core electrons but also valence electrons and chemical bonds. Extensive experimental studies have measured the core-electron binding energies of numerous molecules [21, 22] and the recent development of X-ray photoelectron spectroscopy (XPS) has enabled the detailed analysis of the satellites accompanied by the inner-shell ionization [8, 11–13]. The high-resolution XPS has also been applied to observe the vibrational structure to investigate the geometry change and the dynamics in the inner-shell electronic processes [6, 9–17].

The SAC-CI method is useful to study both the main and satellite peaks in the core-electronic spectra as well as valence spectra. In the series of studies [6–18], the SAC-CI method have been successfully applied to the various kinds of core-electron processes; the core-electron binding energies [7]; the inner-shell ionization satellite spectra of CH_4, NH_3 [7], H_2O [11], formaldehyde [8]; and the vibrational spectra of the core-hole state of H_2O [6], CO [10], N_2 [12], CO_2 [14], and N_2O [16]. The g–u splitting of homonucleus molecules like N_2, C_2H_2, C_2H_4, and C_2H_6 has been well predicted [7, 12]. The overlapping vibrational spectra of the low-lying shake-up satellite states of CO [9, 13] and N_2 [12] were also successfully interpreted by the present method; the potential energy curves of the inner-shell shake-up states were accurately calculated. The method has also been applied to the core-electronic excited states [15, 17, 18]. The irregular Rydberg behavior observed for the O1*s* excited states of N_2O [15] and its drastic change due to the ground-state vibrational excitations were clarified [17].

In this section, we briefly review the SAC-CI methodologies for the inner-shell electronic processes and the recent applications to the core-electronic processes like core-electron binding energy, inner-shell shake-up satellite spectrum, vibrational spectrum of main line and satellites, and core-electronic excitation spectrum.

2.1 SAC-CI Methodologies for Inner-Shell Electronic Processes

The SAC-CI method can be applied to the electronic processes in a wide energy region. There are two approaches in SAC-CI for studying the inner-shell electronic processes. One is based on the general-R method [23–25] in which the neutral ground-state Hartree–Fock is adopted for the reference function. The wave function for core ionization, for example, is given by

$$\Psi^{\text{SAC-CI}}_{\text{general}-R} = \left(\sum_{i} R_i + \sum_{ija} R^{a}_{ij} + \sum_{ijkab} R^{ab}_{ijk} + \sum_{ijklabc} R^{abc}_{ijkl} + \cdots \right) \exp\left(\sum_{I} S_I \right) \Phi_{HF}, \tag{1}$$

where R and S represent the operators in the SAC-CI expansion and Φ_{HF} is the closed-shell ground-state Hartree–Fock. In this method, the higher-order R-operators such as triples and quadruples are necessary for describing both orbital relaxation and electron correlations of the core-electronic processes. Although the SD-R method is accurate for the one-electron processes of the valence excitations and ionizations, higher-order operators are indispensable for the core-electronic processes. For example, for calculating the core-electron binding energy, R-operators up to triples are necessary and for the shake-up satellite states, the SDTQ-R calculations are required. One-rank higher operator is necessary for describing large orbital relaxation in the calculation of the core-electronic processes. Thus, this method is simple and accurate, but, its computational cost is relatively high since it usually includes higher operators for the accurate calculations. Nonetheless, this method is useful since it can be applied to the general core-electronic processes like the g–u splitting in the molecules with equivalent atoms.

The other approach is the open-shell reference (OR) SAC-CI method [26], in which the core-ionized ROHF is used for the reference:

$$\Psi^{\text{OR-SAC-CI}}_{\text{SD}-R} = \left(\sum_{i} R_i + \sum_{ija} R^{a}_{ij} \right) \Psi^{\text{OR-SAC}}, \tag{2}$$

$$\Psi^{\text{OR-SAC}} = \exp\left(\sum_{I} S_I \right) \exp\left(\sum_{J} S'_J \right) O_K \Phi_{HF}, \tag{3}$$

where $O_K \Phi_{HF}$ represents the core-hole ROHF. The S and S' operators are the excitation and de-excitation operators, respectively. Since the OR-SAC-CI method starts from the core-hole state, the method is efficient and accurate; the SD-R method is sufficient for describing the core-hole state. However, it introduces the complex expansion of the wave function due to the de-excitation operators. For applying the g–u splitting of the molecules with equivalent atoms, the accurate calculations including higher-order product terms are necessary since it starts from the different reference functions for g and u states.

In the present applications, the former type of the method, the SAC-CI general-R method, has been adopted and applied to the various kinds of the core-electronic processes.

2.2 Core-Electron Binding Energies

For the theoretical study on the core-electron binding energy, the pioneering works have been performed by the ΔSCF and DFT methods [27–29], however, the accurate prediction is still difficult. The SAC-CI method has been systematically applied to the core-electron binding energies of the C, N, O, and F ionizations of 22 molecules [7]. For calculating the core-electron binding energy based on the method starting from the neutral ground-state reference function, the R-operators up to triples are necessary for describing orbital relaxations as well as electron correlations. In Fig. 1, we show a comparison between the theoretical and experimental values for

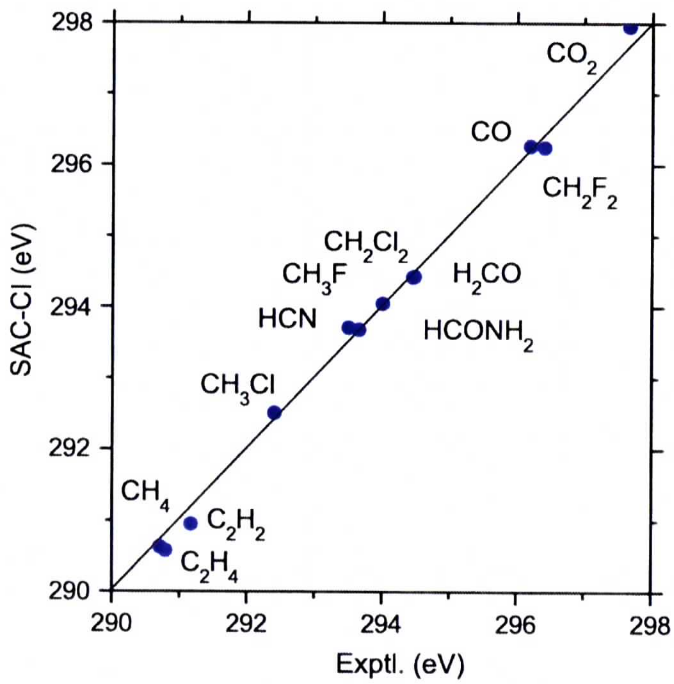

Fig. 1 C1*s* core-electron binding energy [7]

the C1*s* ionizations of 12 molecules. The SAC-CI SDT-*R* method calculated the core-electron binding energies of these molecules quite accurately. In general, the core-electron binding energy shifts into higher energy, when the adjacent atom is electron withdrawing. The SAC-CI method reproduced this chemical shift accurately and the averaged absolute deviation from the experimental values was 0.13 eV for these molecules.

2.3 Vibrational Spectra of Core-Hole States

In the core-electron processes, the reorganization of the electron distribution affects the valence electrons and the characteristic geometry change usually occurs. This geometry change can be observed in the vibrational spectrum. Vibrationally resolved C1*s* and O1*s* photoelectron spectra of carbon monoxide have been measured by the high-resolution X-ray photoelectron spectroscopy. To understand the physics in the vibrational spectra, the potential energy curves of the ground and C1*s* and O1*s* core-ionized states were calculated and the vibrational analysis was performed with the grid method [10]. These vibrational spectra were also studied by the Green's function method [30]. The experimental and theoretical vibrational spectra for the C1*s* and O1*s* ionizations are compared in Fig. 2. The geometry changes and the Franck Condon factors (FCF) are summarized in Tables 1 and 2, respectively. In the C1*s* ionized state, the CO bond shrinks by $\Delta R = -0.051$ Å, while the CO bond length in the O1*s* ionized state was predicted to become longer by $\Delta R = +0.028$ Å. The bond shrink in the C1*s* ionization can be explained by the enhancement of the charge distribution $C^{\delta+}$–$O^{\delta-}$. On the other hand, the O1*s* ionization causes the Coulomb repulsion described by $C^{\delta+}$–$O^{\delta+}$ and results in the CO bond elongation. Although the FCF is the sensitive quantity, the calculated FCF satisfactorily agrees with those extracted from the experimental spectra in the sudden limit as shown in Table 2.

2.4 Inner-Shell Shake-Up Satellite Spectra

Shake-up satellites that appear in the photoelectron spectra are challenging spectroscopic subject from both theoretical and experimental viewpoints. Theoretically, a precise description of the satellite states is possible only with advanced theoretical methods because the spectra reflect very complex electron-correlation and orbital-reorganization effects. Experimentally, the weak intensities of photoelectron satellites make high-resolution photoelectron spectroscopy difficult. In this section, we show the cooperative study by the SAC-CI and XPS on the inner-shell satellite spectra of CO [13]. In these spectra, the valence and Rydberg excitations accompanying the inner-shell ionizations make the satellite spectra complex. Therefore, the

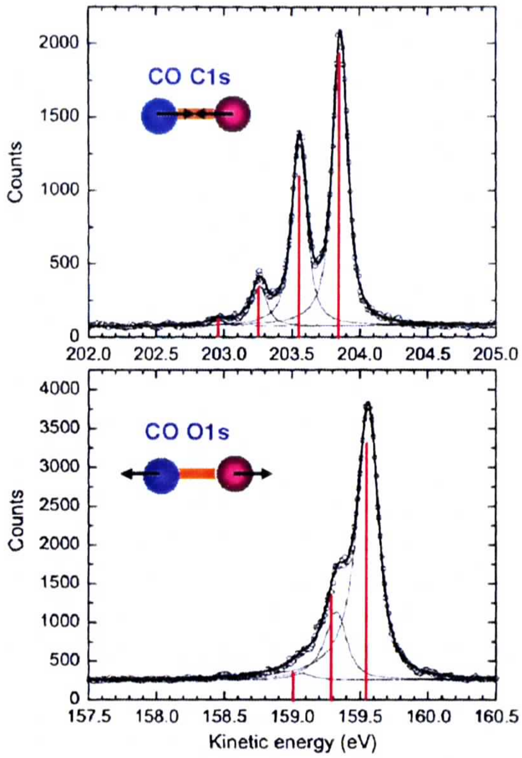

Fig. 2 Vibrational spectra of C1*s* and O1*s* ionizations of CO. The SAC-CI spectra are shown with the *vertical lines* [10]

Table 1 Geometry and harmonic frequency of the C1*s* and O1*s* ionized states of CO [10]

	C1*s*		O1*s*	
	Exptl.	SAC-CI	Exptl.	SAC-CI
R_e (Å)	1.077	1.075	1.165	1.156
ΔR_e (Å)	−0.051	−0.051	+0.037	+0.028
ω_e (cm^{-1})	2479	2444	1864	1928

Table 2 Franck–Condon factors of the C1*s* ionizations of CO [10]

Transition	Exptl.	SAC-CI
0–0	1.000	1.000
0–1	0.637	0.628
0–2	0.154	0.134
0–3	0.019	0.012

accurate theoretical study of these spectra in a wide energy region is challenging [31, 32].

Figure 3 shows the observed XPS and the SAC-CI general-*R* spectra of the C1*s* satellites of CO. The SAC-CI method satisfactorily reproduces the shape of the

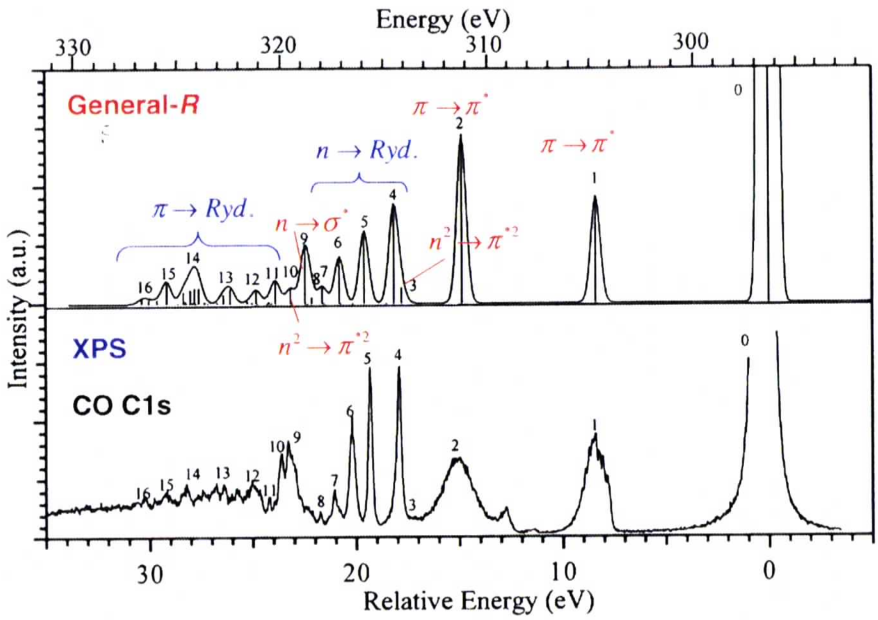

Fig. 3 C1s shake-up satellite spectrum of CO [13]

experimental satellite spectrum, although the intensity of the XPS does not necessarily agree with the theoretical monopole intensity. For reproducing the inner-shell satellite spectrum, it is necessary to include R-operators up to quadruples, that is the SDTQ-R calculations: the conventional SAC-CI SD-R method gives errors beyond 10 eV for these satellites and even qualitative assignment is impossible. The SAC-CI SDTQ-R spectrum enabled the reliable assignments for the 16 satellite bands. The satellite band 1 was assigned to the $\pi\pi^*$ shake-up state, while the strongest band 2 was the $\pi\pi^*$ shake-up state strongly interacting with the three-electron processes like $C1s^{-1}\pi^{-2}\pi^{*^2}$. Weak satellite peak 3 is also assigned to the double excitation, $n^{-2}\pi^{*^2}$ transition. The continuous sharp peaks above peak 4 in the higher energy region are dominantly assigned to the numerous Rydberg transitions.

In contrast to the C1s satellite spectrum, theoretical analysis of the O1s satellite spectrum has been very limited. Like formaldehyde, the O1s satellite spectrum has different characteristics from the C1s spectrum. The different features of these spectra can be interpreted in terms of charge reorganization. The comparison with the experimental and theoretical spectra was made in Fig. 4. The accurate theoretical prediction of the O1s satellite spectrum is difficult since most of the satellite states are contributed by the three-electron processes. Peaks 1 and 2 are assigned to the $\pi\pi^*$ state and have the significant contribution of three-electron process $\pi^{-2}\pi^{*^2}$ compared to the C1s ionization. Peaks 3–9 are characterized as $5\sigma\sigma^*$ or $5\sigma n\sigma$ transitions interacting with the three-electron process of $n^{-2}\pi^{*^2}$ and $\pi^{-2}\pi^{*^2}$

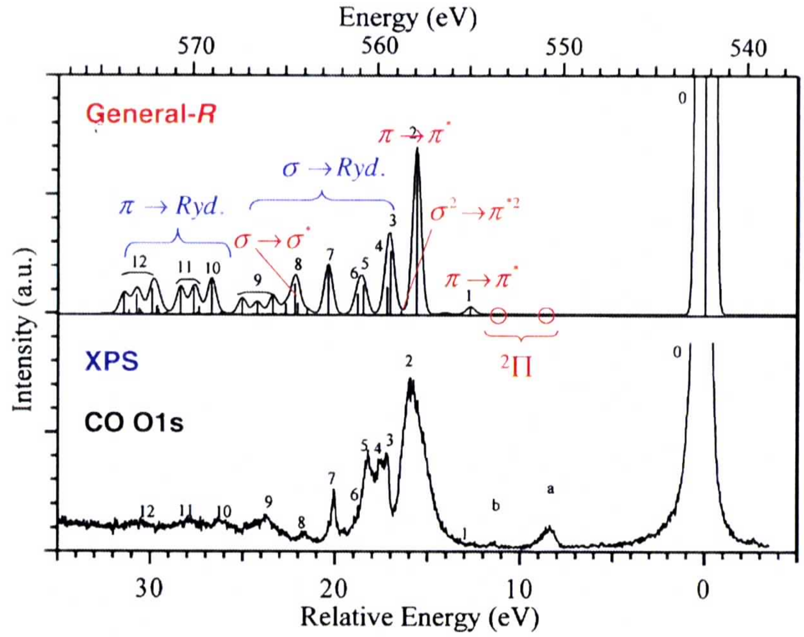

Fig. 4 O1*s* shake-up satellite spectrum of CO [13]

configurations. The broad continuous bands in the higher energy region are dominantly assigned to the transitions to the Rydberg orbitals.

2.5 Geometry Changes and Vibrational Spectra of Inner-Shell Shake-Up Satellites

For the C1*s* shake-up satellite peak at 8–9 eV above the mainline of CO, the angle-resolved ion-yield (ARIY) spectroscopy was applied to observe the vibrational structure. By measuring at the two different angles 0° and 90° relative to the polarization vector, space symmetry of the electronic states can be resolved; the measurement at 0° mainly observes the direct shake-up in Σ symmetry, while the measurement at 90° observes the conjugate shake-up in Π symmetry. However, since the Σ and Π states interfere with each other at the polarization angle of 0°, the separation of the symmetry is not complete in the spectrum at the measurement of 0°. Therefore, we decomposed the overlapping spectra using the SAC-CI calculations [9, 13].

We calculated the potential energy curves of the shake-up satellites in this energy region. Figure 5 shows the SAC-CI SDTQ-*R* potential energy curves of these satellites. One Σ^+ state and two Π states were found to exist in this energy region and the Δ and Σ^- states were also located in the higher region. The geometry change in the Σ^+ state is large since this state is characterized as the π–π^* excitation accompanied by the C1*s* ionization. On the other hand, two Π states are n–π^* transition and therefore, the structure relaxation of these two states is small. The Δ and Σ^-

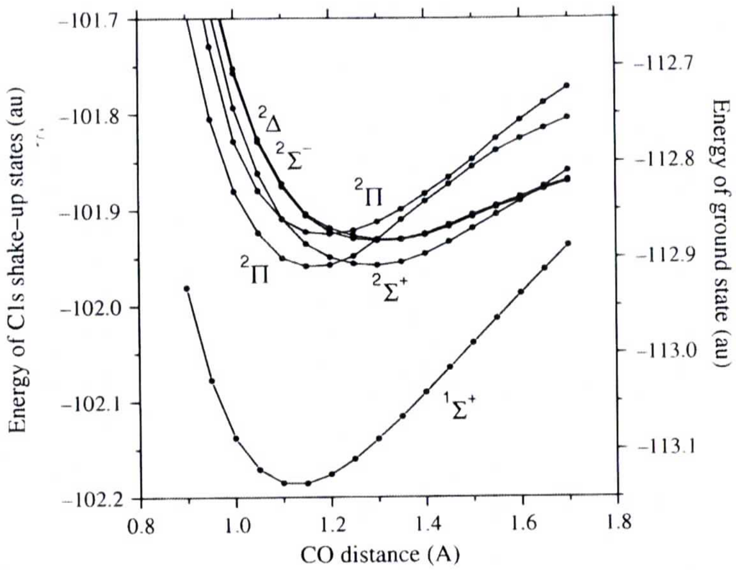

Fig. 5 Potential energy curves of the ground and C1*s* shake-up satellite states of CO calculated by the SAC/SAC-CI method [9]

states have the same character as the Σ^+ state and the potential curves of these states are very similar to that of the Σ^+ state.

Vibrational analysis was performed with the potential energy curves in Fig. 5. Figure 6 shows the theoretically decomposed vibrational spectra; the experimental spectra were successfully decomposed into one Σ^+ state and two Π states. Calculating the accurate vibrational spectra of the Σ and Π states theoretically, the experimental Σ spectrum was obtained as $I(0)–c \times I(90)$, where $I(0)$ and $I(90)$ are the spectral distributions of the 0° and 90° measurement, respectively, and c=0.4 was selected with the help of the SAC-CI calculations. The satellite Σ^+ state shows the excitation to the high vibrational levels reflecting the large geometry change, while the vibrational excitations are not prominent in the two Π states. The vibronic coupling is sometimes relevant for the core-ionized states. In the present case, two Π states are relatively separated in the FC region and the independent vibrational analysis for each state is reasonable. The Δ and Σ^- states may contribute to the higher energy region of the band, but they are not prominent.

2.6 Strong Valence–Rydberg Coupling in Inner-Shell Excited States

ARIY spectra were also measured in the O K edge of N_2O [15]. The first ARIY spectra of N_2O were investigated in 1995 with the help of *ab initio* calculations [33]. Figure 7 shows the ARIY spectra measured at the angles of 0° and 90° compared

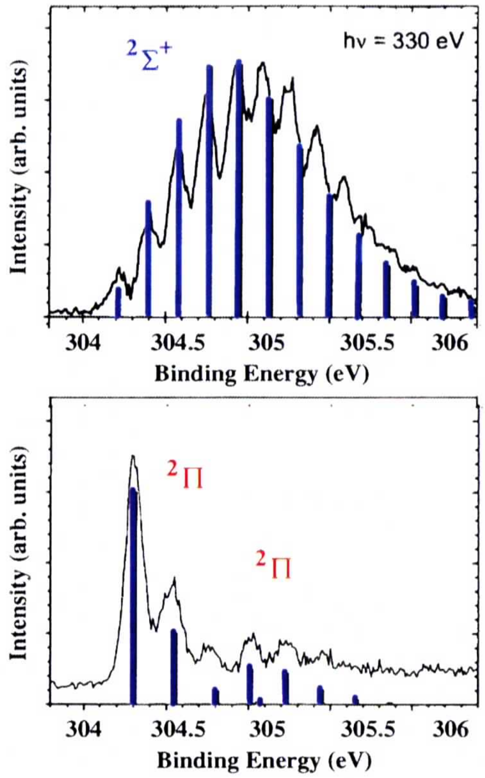

Fig. 6 Vibrational spectra of the C1*s* shake-up satellite states of CO decomposed by the SAC-CI method [9]. The SAC-CI spectrum was shown with the *vertical lines*

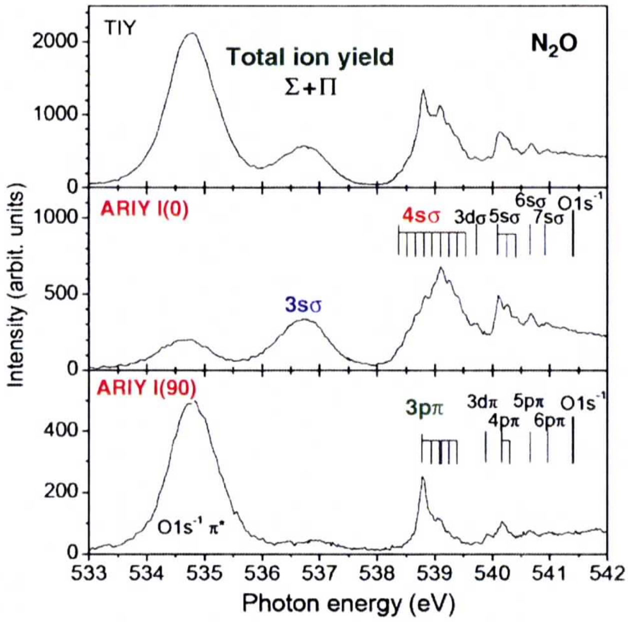

Fig. 7 Angle-resolved ion-yield (ARIY) spectra of O1*s* excitations of N_2O measured at 0° and 90° compared with the total ion-yield (TIY) spectrum [15]

with the total ion-yield measurement. The measurement at 0° mainly observes the Σ states, while the measurement at 90° observes Π states. As shown in Fig. 7, in the Rydberg 4*sσ* state, irregular excitation to the higher vibrational levels was observed [15].

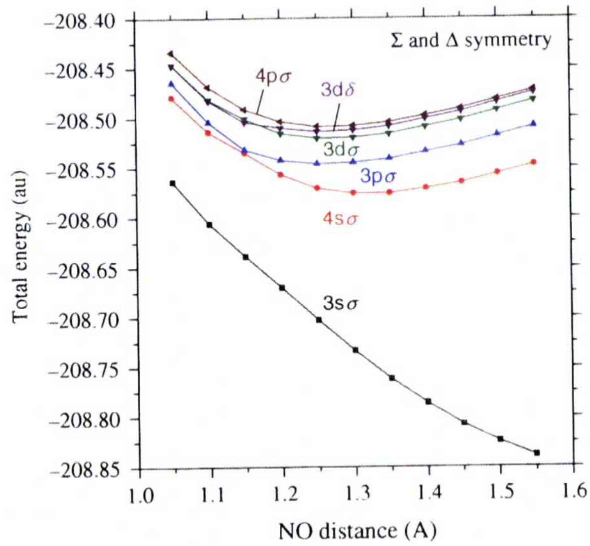

Fig. 8 Potential energy curves of the O1s excited states of N_2O with the cut of $R_{NN} = 1.1$ Å [15]

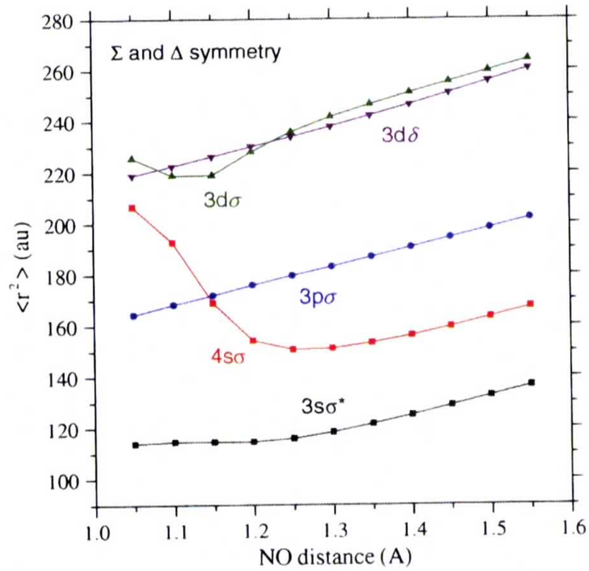

Fig. 9 Electronic part of the second moments $< r^2 >$ of the O1s excited states of N_2O with the cut of $R_{NN} = 1.1$ Å [15]

For clarifying this irregular vibrational progression, the potential energy surfaces of the O1s core-excited states were examined [15]. In the SAC-CI calculations, the equivalent-core approximation was adopted and the direct SAC-CI algorithm [34] was used. Figures 8 and 9 show the potential energy curves and the electronic part of the second moments $<r^2>$, respectively, for the O1s excited states in Σ and Δ symmetry along the R_{NO} distance. The second moment $<r^2>$ of the 4$s\sigma$ state drastically decreases in the large R_{NO} distance and this shows that the strong valence–Rydberg coupling occurs in the 4$s\sigma$ state having σ* component. Due to this strong valence–Rydberg coupling, the 4$s\sigma$ state has the potential minimum at large

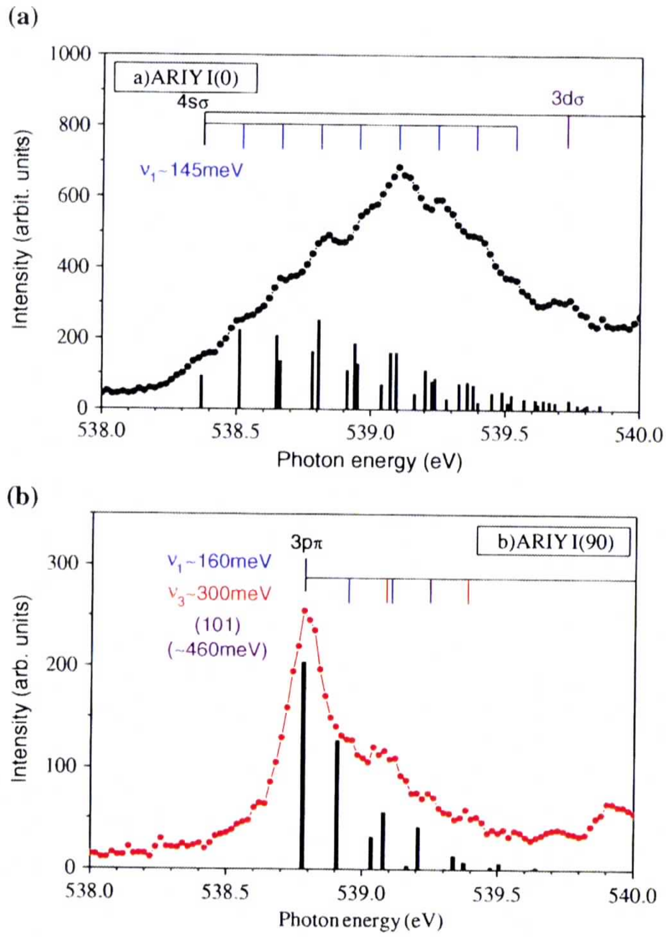

Fig. 10 Vibrational spectra of (a) O1s–4$s\sigma$ and (b) O1s–3$p\pi$ excited states of N_2O. The SAC-CI spectra are shown by the *vertical solid lines* [15]

R_{NO} distance. Thus, we conclude that the irregular Rydberg behavior in the 4$s\sigma$ state is caused by the strong valence–Rydberg coupling.

Based on the SAC-CI two-dimensional potential energy surfaces, Franck–Condon analysis was performed for the 4$s\sigma$ and 3$p\pi$ states. Theory reproduced the observed vibrational excitations satisfactorily as shown in Fig. 10. The higher vibrational levels are excited in the 4$s\sigma$ state, while the vibrational spectrum of the 3$p\pi$ state shows the standard Rydberg-type vibrational progression. For the deviation of the 4$s\sigma$ state, the 3$p\sigma$ state may contribute to the higher energy region and the vibronic coupling among these states is important.

2.7 Thermal Effect in Inner-Shell Excitation Spectra

Absorption spectra of the vibrationally excited "hot" molecules were observed for the O1s excitations of N_2O. The absorption spectra were measured at 300/700 K and

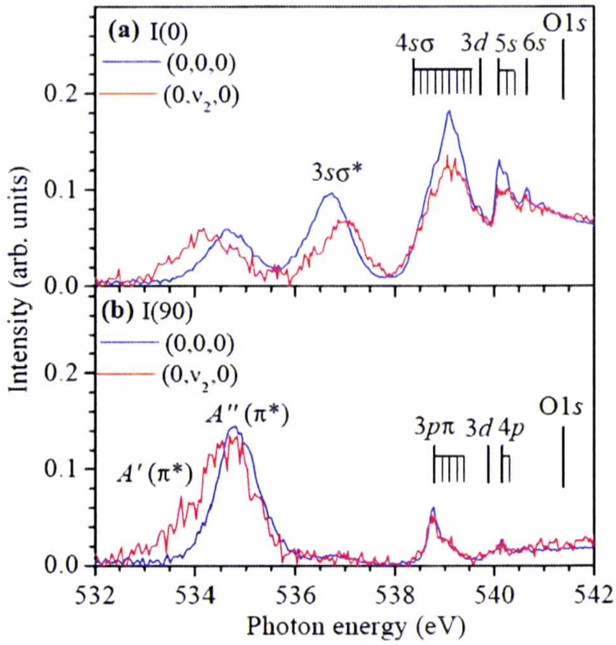

Fig. 11 ARIY spectra in the N_2O O1*s* excitation region: *blue* and *red lines* show the spectra from vibrationally ground and excited states, respectively [17]

the vibrationally excited absorption spectrum was extracted assuming the Boltzmann distribution (Fig. 11) [17]. Comparing the spectra of (0,0,0) and (0,v_2,0), the intensity of the $ns\sigma$ Rydberg series is significantly suppressed, while that of the $A'(\pi)$ state is enhanced in the excitation from the vibrationally excited states (0,v_2,0). These observations suggest that the decrease in the bond angle causes a decrease in the mixing of the valence character that enhances the transition probability to the Rydberg states. Energy shift was also observed in the spectra from the vibrationally excited states.

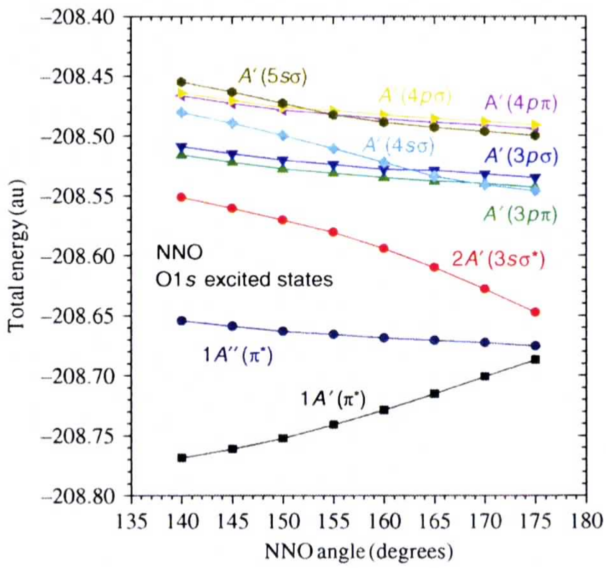

Fig. 12 Potential energy curves of the low-lying O1*s* excited states of N_2O along the bending coordinate [17]

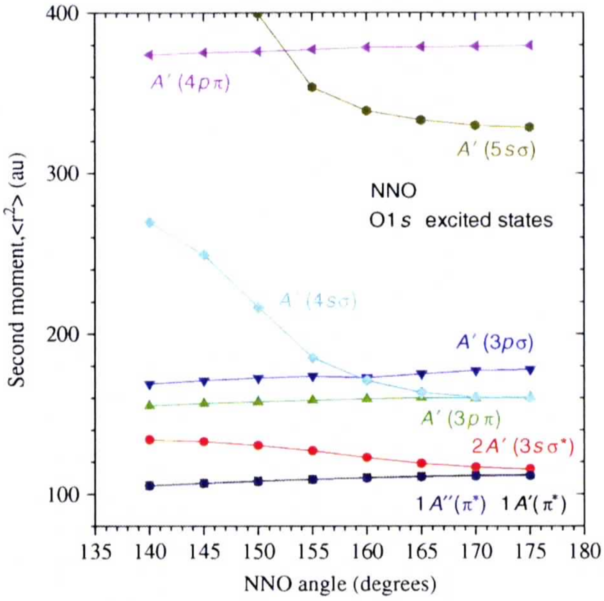

Fig. 13 Electronic part of the second moments $<r^2>$ of the low-lying O1*s* excited states of N_2O along the bending coordinate [17]

In order to understand these phenomena, we executed the SAC-CI calculations of the energies and the second moment $<r^2>$ of the O1*s* excited states varying the bond angle [17]. Figure 12 shows the cuts of the calculated potential energy surfaces of the O1*s* excited states of A' symmetry. The $1A'$ state correlates with the π^* state and stabilizes along the bending coordinate. All other states are stable in the linear structure. A characteristic curve crossing occurs between the σ and π Rydberg states along the bending coordinate. These potential curves explain the red shift of the π^* state and the blue shift of $3s\sigma$ and $4s\sigma$ states. In order to analyze the mixing of the valence character in the Rydberg states, we examined the second moment $<r^2>$, which is anticorrelated with the amount of valence character (Fig. 13). The second moments of the $3s\sigma$, $4s\sigma$, and $5s\sigma$ states become large as the molecule becomes bent. This indicates that the mixing of the valence character in these states becomes less as the bond angle decreases. Consequently, the absorption oscillator strength to the $ns\sigma$ Rydberg states becomes small. These results confirm the interpretation of the intensity changes observed for excitation from vibrationally excited molecules.

As seen in Fig. 12, the $A'(\pi^*)$ state stabilizes along the bending coordinate, whereas the $3sA'$ state destabilizes more than the $A''(\pi^*)$ state. This anticorrelation indicates that the $A'(\pi^*)$ and $3sA'$ states are strongly coupled. This coupling opens a flow of the valence character from the $3sA'$, $4sA'$, and $5sA'$ Rydberg states to the $A'(\pi^*)$ state. Analyzing the MOs which contribute to the excitations, we concluded that the counterpart of the decrease in the mixing of the valence character in the 3*s*, 4*s*, and 5*s* states is an increase in the $s\sigma$-type character of the $a'(\pi^*)$ orbital.

Based on the SAC-CI calculations of the electronic part of the second moment $<r^2>$, the suppression is interpreted as being due to a decrease in the mixing of the valence character in the $ns\sigma$ Rydberg states with decreasing bond angle.

3 Photochemistry of Organic Light-Emitting Diodes and Biological Chemosensor

Organic light-emitting diodes are one of the promising candidates for the next generation electro-optical devices such as panel display. Theoretical prediction of the photo-physical properties of the OLED is relevant for the molecular design. The excited-state chemistry of the OLED contains the interesting issue like localization/delocalization of the excitation and the effect of the flexible conformation. We have studied the absorption and emission spectra and the excited-state dynamics of some OLED molecules like poly *para*-phenylene vinylene [19] and fluorene-thiophene [20].

The biological chemosensor has also been focused and extensively investigated since they enable the direct detection of the physiologically active substances in cell and real-time monitoring of enzyme activities without influencing the proteins so much. The photochemistry of some fluorescent probes is interesting since they are controlled by the photo-induced electron transfer. We have investigated the photochemistry of the biological chemosensor which probes the anion species.

3.1 Electronic Spectra and Excited-State Geometries of Poly Para-Phenylene Vinylene

The optical properties of poly *para*-phenylene vinylene (PPV) that is well known as an efficient light emitter have been extensively investigated [35–40], however, the accurate theoretical prediction of the transition energies is still challenging. The electronic spectra and excited-state geometries of the PPV oligomer (Fig. 14) were investigated by the SAC-CI SD-R method. The calculated absorption and emission energies of the lowest singlet excited state of PPVn ($n = 1$–4) are compared with the experimental values [36] and other theoretical values [37, 38] in Fig. 15. The SAC-CI method predicted the experimental values in high accuracy; the mean deviations are 0.09 eV for absorption and 0.03 eV for emission. The method reproduced the chain length dependence of the excitation energy better than the TDDFT/B3LYP calculations. The conventional TDDFT should be carefully used for the transition energies of the molecules with long π-conjugated chains.

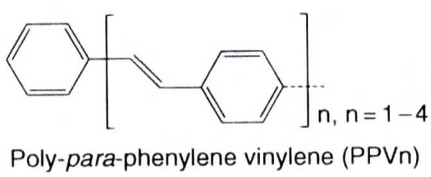

Fig. 14 Molecular structure of PPVn oligomer

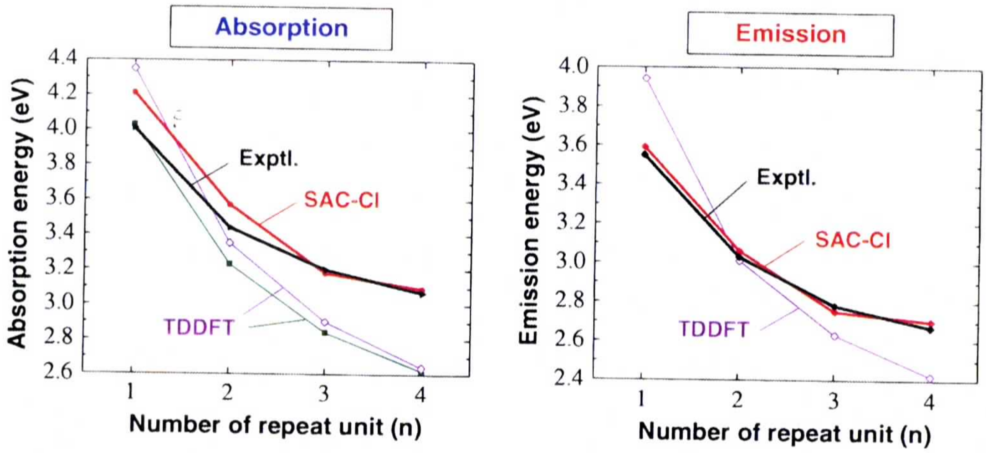

Fig. 15 Excitation (*left*) and emission (*right*) energies of the S_1 state of PPVn (n=1–4) plotted to the repeat unit n [19]

The ground-state and lowest singlet (S_1) and triplet (T_1) excited-state structures of PPVn were calculated to be planar by the SAC-CI method. The calculated ground-state geometry agrees very well with the experimental values; the deviations are within 0.005 Å and 0.07° for the bond length and bond angle, respectively, for PPV1. The changes in bond length (Δr) along the CC conjugation due to singlet and triplet excitations of PPV1 are shown in Fig. 16. In the S_1 and T_1 states, the central vinylene C=C bond length increases, whereas the vinylene C–C bond length

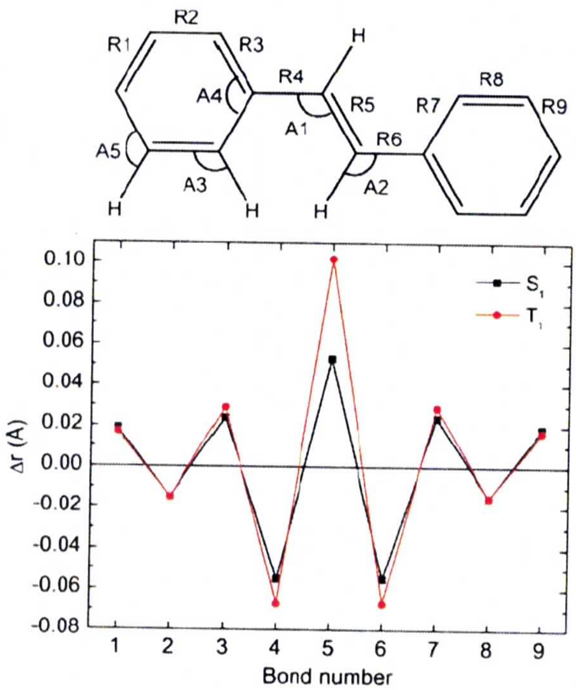

Fig. 16 CC bond length changes in the S_1 and T_1 states of PPV1 [19]

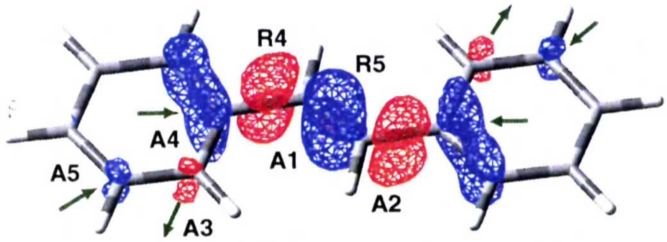

Fig. 17 Electron density difference between the S_0 and S_1 states calculated by the SAC/SAC-CI method [19]

decreases. These changes are localized in the central part of the PPVn oligomers. The bond length alternation changes significantly in the excited states from that of the ground state. Larger bond length changes were obtained for the T_1 state than for the S_1 state.

These changes in the geometry due to excitation can be explained using the electrostatic force (ESF) theory [41, 42]. In ESF theory, the geometric relaxation in the excited state can be explained by the force acting on nuclei caused by changes in the electron distribution. Molecular shape in the ground and excited states is determined by the balance of the atomic dipole (AD), exchange (EC), and gross charge (GC) forces. The SAC/SAC-CI electron density difference between the ground and S_1 states due to excitation of PPV1 is shown in Fig. 17. The electron density in the central vinylene C=C bond region decreases and that in the vinylene C–C bond region increases. More precisely, the electron density in the σ-bond region increases and that in the π-bond region decreases; this is a general trend in these PPVn molecules. The EC force along the central vinylene C=C bond decreases because of the decrement of electron density in the C=C bond region, whereas the EC force is enhanced along the vinylene C–C bond. Consequently, the central vinylene C=C bond length increases and the vinylene C–C bond length decreases. The accumulations (depletions) of electron density in the vicinity of C nuclei also explain the bond angle change in the excited states. For example, in PPV1, angle A3 (Fig. 17) is enlarged in the singlet excited state (119.4°) from that in the ground state (118.3°) as a result of an accumulation of electron density in the region of the associated C nucleus.

3.2 *Conformational Effect of Fluorene-Thiophene and Its Derivative on Electronic Spectra*

The fluorene co-polymers constitute rigorous candidates for the flexible and tunable light-emitting diodes [43–45]. By introducing the suitable substituents, the optical properties can be controlled because of its flexible structure. In particular, fluorene-thiophene co-polymers have been focused since they are the candidates for the

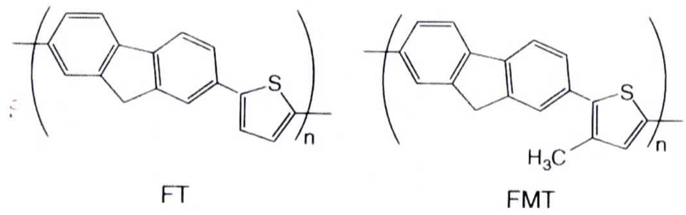

Fig. 18 Molecular structures of the FT and FMT oligomers

blue-light emitter. The unit of these co-polymers, fluorene-thiophene (FT), and fluorene-methyl-thiophene (FMT) (Fig. 18) show the characteristic electronic spectra [43]. The energy region of the absorption spectrum is almost the same; however, the shape of the electronic spectra of these molecules is different. To interpret the difference of the spectra, the ground and excited states of these molecules and the conformational effect on the electronic spectra were investigated by the SAC-CI method [20]. The FT and FMT monomers were examined for elucidating the essence of the spectrum shape, and the electronic spectra up to trimers were calculated.

The ground-state potential energy curves of the FT and FMT monomers along the torsion angle are shown in Fig. 19. The dihedral angles of the most stable conformation of FT and FMT are $\theta = 27°$ and 43°, respectively. These molecules have very flexible structure with regard to the torsion. The potential energy curves are very flat for the torsion; the relative energy of the conformers for $\theta = 0°–60°$ is within about 1.0 kcal/mol. This low rotational energy barrier indicates that it allows a wide range of nonplanar conformation of these molecules at room temperature.

The optical properties of the low-lying excited states of these molecules are dependent on the torsion angle. The excitation energy and oscillator strength as the function of the torsion angle are displayed in Fig. 20. The first to third excited states interact with each other along the torsion. The avoided crossing occurs between the first and third excited states in the region of $\theta = 30–60°$; this interaction is clearly seen in the oscillator strength.

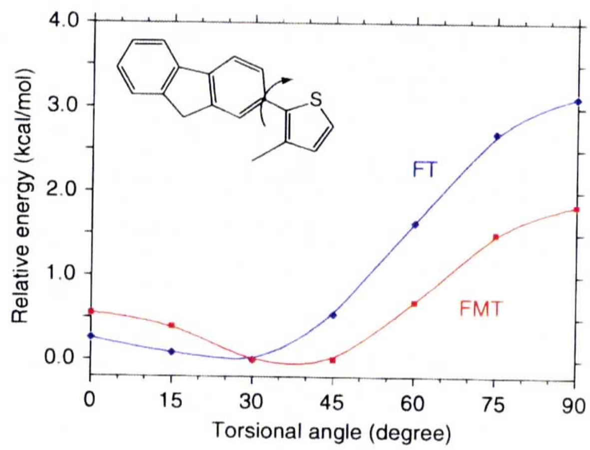

Fig. 19 The ground-state potential energy curves of the FT and FMT monomers [20]

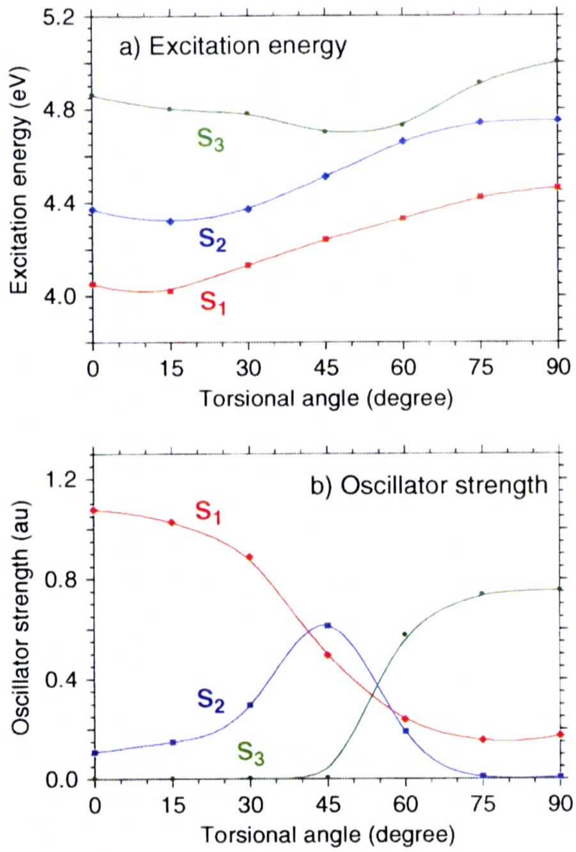

Fig. 20 SAC-CI (**a**) excitation energy and (**b**) oscillator strength of the lowest three excited states of FT versus torsion angle [20]

Since the ground-state potential energy surfaces are flat for the torsion and the excitation spectra are dependent on this coordinate, thermal average of the conformers should be considered in order to simulate the absorption spectra. The simulated absorption spectra of FT and FMT, in which thermal distribution at 298 K is taken into account, are compared with the experimental spectra in Fig. 21. The simulated spectra with thermal average showed excellent agreement with the experimental spectra. For FT, the contribution of the conformer whose torsion angle is up to $\theta = \sim 30°$ is dominant and the asymmetric spectrum is obtained. In the case of FMT, the strong shoulder was measured in the higher energy side of the peak. This shoulder is attributed to the second excited state of the conformer of θ=30–45°.

The SAC-CI calculations show that the thermal average of the conformers is important to interpret the electronic spectra of the fluorene-thiophene co-polymer.

3.3 *Photochemistry of Biological Chemosensor*

The fluorescent artificial chemosensor has been focused since they can directly detect the physiological active substances in cell and enables real-time monitoring of enzyme activities. In this field, probes of anions are the most relevant and

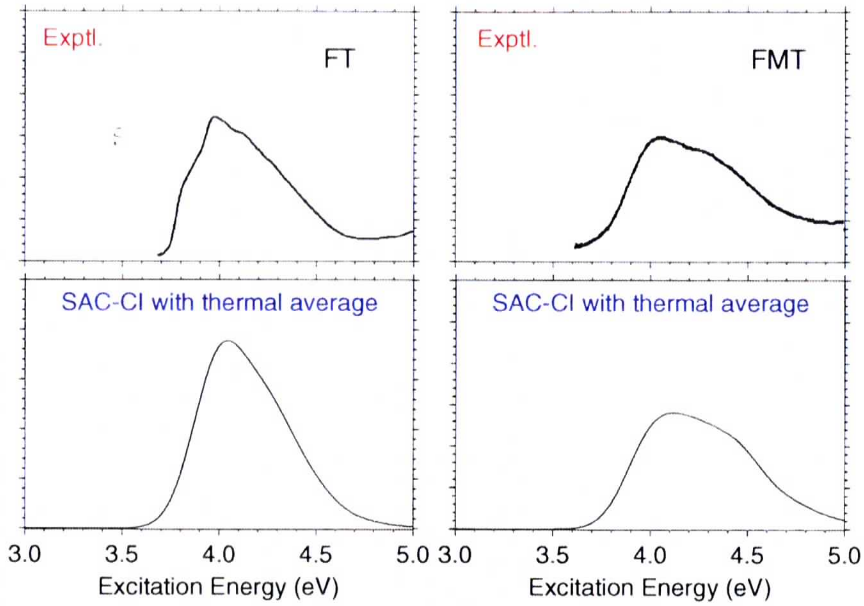

Fig. 21 Experimental and SAC-CI absorption spectra of FT and FMT [20]

difficult issue. Recently, novel molecular fluorescent probes which can selectively recognize the phosphodiesters have been developed [46, 47]. One of these fluorescent probes, acridine-based probe, shows drastic fluorescence change in the presence of Zn^{2+} ion. The photochemistry of this acridine-based fluorescent probe has been investigated by the SAC-CI method, in particular for the electronic mechanism of the photo-induced electron transfer and the origin of the energy shift in the fluorescence. First, the stable structures of the mono-nuclear and bi-nuclear Zn(II) complexes were determined with the density functional theory. The fivefold structure was most stable for the mono-nuclear complex and threefold+threefold structure was stable for the bi-nuclear complex. The fluorescence of this probe molecule is controlled by the photo-induced electron transfer. For the photo-induced electron transfer, relative energy of the charge transfer state and $\pi\pi^*$ excited state is very important. The solvation effect and the geometry relaxation were found to be relevant for these states. These two factors control the photo-induced electron transfer of this fluorescent probe. Characteristic energy shift of the fluorescence was found to be determined by the location of the Zn(II) ion in the fluorescent acridine unit.

4 Summary

The SAC-CI method has been applied to the theoretical spectroscopy of the inner-shell electronic processes and the photochemistry of the organic light-emitting diodes and biological chemosensor.

Various kinds of the core-electronic processes such as core-electron ionizations, shake-up satellites, vibrational excitations, and valence–Rydberg coupling have been investigated by the SAC-CI general-R method. The general-R method calculated the core-electron binding energies and the shake-up satellite spectra very accurately. The method also predicted the geometry changes of the core-hole states and the shake-up satellites and reproduced the vibrational spectra of these states. The irregular vibrational progressions observed in the O1s–4$s\sigma$ excited state of N_2O and the thermal effect of the O1s absorption spectra were elucidated in terms of the valence–Rydberg coupling.

The SAC-CI method has also predicted the absorption and emission spectra of the organic light-emitting diodes in high accuracy. The geometry changes in the excited states of PPV were interpreted with the ESF theory. For FT and FMT, the thermal average was shown to be important to simulate the electronic spectra. The method clarified the electronic mechanism of the photo-induced electron transfer of the acridine-type fluorescent probe. The solvation effect and geometry relaxation in the charge transfer state and the $\pi\pi^*$ excited state were found to be essential.

Acknowledgments The authors are grateful to Prof. K. Ueda for the works on the inner-shell electronic processes, to Drs. B. Saha, P. Poolmee, and S. Hannongbua for the works of OLED, and to Prof. I. Hamachi and Dr. A. Ojida for the work on biological chemosensor. This study was supported by JST, CREST, and a Grant-in-Aid for Scientific Research in Priority Areas "Molecular Theory for Real Systems" from the Ministry of Education, Culture, Sports, Science and Technology of Japan.

References

1. H. Nakatsuji, Chem. Phys. Lett. **59**, 362 (1978)
2. H. Nakatsuji, Chem. Phys. Lett. **67**, 329 (1979)
3. H. Nakatsuji, *SAC-CI method: Theoretical Aspects and Some Recent Topics*, in *Computational Chemistry, Review of Current Trends*, ed. by J. Leszczyński (World Scientific, Singapore, 1997), Vol. 2, p. 62
4. M. Ehara, J. Hasegawa, H. Nakatsuji, *SAC-CI Method Applied to Molecular Spectroscopy*, in *Theory and Applications of Computational Chemistry: The First 40 Years*, eds. by C.E. Dykstra, G. Frenking, K.S. Kim, G. E. Scuseria (Elsevier, Oxford, 2005), p. 1099
5. M. J. Frisch et al., *GAUSSIAN03* (Gaussian Inc., Pittsburgh, PA, 2003)
6. R. Sankari, M. Ehara, H. Nakatsuji, Y. Senba, K. Hosokawa, H. Yoshida, A.D. Fanis, Y. Tamenori, S. Aksela, K. Ueda, Chem. Phys. Lett. **380**, 647 (2003)
7. K. Kuramoto, M. Ehara, H. Nakatsuji, J. Chem. Phys. **122**, 014304 (2005)
8. K. Kuramoto, M. Ehara, H. Nakatsuji, M. Kitajima, H. Tanaka, A.D. Fanis, Y. Tamenori, K. Ueda, J. Electron Spectrosc. Relat. Pheonom. **142**, 253 (2005)
9. K. Ueda, M. Hoshino, T. Tanaka, M. Kitajima, H. Tanaka, A.D. Fanis, Y. Tamenori, M. Ehara, F. Oyagi, K. Kuramoto, H. Nakatsuji, Phys. Rev. Lett. **94**, 243004 (2005)
10. M. Matsumoto, K. Ueda, E. Kukk, H. Yoshida, T. Tanaka, M. Kitajima, H. Tanaka, Y. Tamenori, K. Kuramoto, M. Ehara, H. Nakatsuji, Chem. Phys. Lett. **417**, 89 (2006)
11. R. Sankari, M. Ehara, H. Nakatsuji, A.D. Fanis, S. Aksela, S.L. Sorensen, M.N. Piancastelli, K. Ueda, Chem. Phys. Lett. **422**, 51 (2006)

12. M. Ehara, H. Nakatsuji, M. Matsumoto, T. Hatamoto, X.-J. Liu, T. Lischke, G. Prümper, T. Tanaka, C. Makochekanwa, M. Hoshino, H. Tanaka, J.R. Harries, Y. Tamenori, K. Ueda, J. Chem. Phys. **124**, 124311 (2006)
13. M. Ehara, K. Kuramoto, H. Nakatsuji, M. Hoshino, T. Tanaka, M. Kitajima, H. Tanaka, Y. Tamenori, A.D. Fanis, K. Ueda, J. Chem. Phys. **125**, 114304 (2006)
14. T. Hatamoto, M. Matsumoto, X.-J. Liu, K. Ueda, M. Hoshino, K. Nakagawa, T. Tanaka, H. Tanaka, M. Ehara, R. Tamaki, H. Nakatsuji, J. Electron Spectrosc. Relat. Phenom. **155**, 54 (2007)
15. T. Tanaka, R. Feifel, H. Tanaka, M. Hoshino, M. Kitajima, L. Karlsson, K. Ueda, M. Ehara, R. Fukuda, R. Tamaki, H. Nakatsuji, Chem. Phys. Lett. **435**, 182 (2007)
16. M. Ehara, R. Tamaki, H. Nakatsuji, R. R. Lucchese, J. Soderstrom, T. Tanaka, M. Hoshino, M. Kitajima, H. Tanaka, A. D. Fanis, K. Ueda, Chem. Phys. Lett. **438**, 14 (2007)
17. T. Tanaka, M. Hoshino, H. Kato, M. Ehara, N. Yamada, R. Fukuda, H. Nakatsuji, Y. Tamenori, J. R. Harries, G. Prümper, H. Tanaka, K. Ueda, Phys. Rev. A **77**, 012709 (2008)
18. M. Ehara, H. Nakatsuji, Coll. Czech. Chem. Commun **73**, 771 (2008)
19. B. Saha, M. Ehara, H. Nakatsuji, J. Phys. Chem. A **111**, 5473 (2007)
20. P. Poolmee, M. Ehara, S. Hannongbua, H. Nakatsuji, Polymer **46**, 6474 (2005)
21. K. Siegbahn, C. Nordling, G. Johansson, J. Hedman, P.-F. Heden, K. Hamrin, U. Gelius, T. Bergmark, L. O. Werme, R. Manne, Y. Baer, *ESCA Applied to Free Molecules* (North-Holland, Amsterdam, 1969)
22. A.A. Bakke, A.W. Chen, W.L. Jolly, J. Electron Spectrosc. Relat. Phenom. **20**, 333 (1980)
23. H. Nakatsuji, Chem. Phys. Lett. **177**, 331 (1991)
24. M. Ehara, H. Nakatsuji, Chem. Phys. Lett. **282**, 247 (1998)
25. M. Ehara, M. Ishida, K. Toyota, H. Nakatsuji, *SAC-CI General-R method: Theory and Applications to the Multi-Electron Processes*, in *Reviews in Modern Quantum Chemistry*, ed. by K.D. Sen (World Scientific, Singapore, 2002)
26. Y. Ohtsuka, H. Nakatsuji, J. Chem. Phys. **124**, 054110 (2006)
27. P.S. Bagus, H. F. Schaefer III, J. Chem. Phys. **55**, 1474 (1971)
28. J.C. Slater, Adv. Quantum Chem. **6**, 1 (1972)
29. D.P. Chong, J. Chem. Phys. **103**, 1842 (1995)
30. A. Thiel, J. Schirmer, H. Köppel, J. Chem. Phys. **119**, 2088 (2003)
31. G. Angonoa, I. Walter, J. Schirmer, J. Chem. Phys. **87**, 6789 (1987)
32. G. Fronzoni, G.D. Alti, P. Devleva, J. Phys. B **32**, 5357 (1999)
33. J. Adachi, N. Kosugi, E. Shigemasa, A. Yagishita, J. Chem. Phys. **102**, 7369 (1995)
34. R. Fukuda, H. Nakatsuji, J. Chem. Phys. **128**, 094105 (2008)
35. J.H. Burroughes, D.D.C. Bradley, A.R. Brown, R.N. Kckay, R.H. Friend, P.L. Burn, A.B. Holmes, Nature **347**, 539 (1990)
36. J. Gierschner, H.-G. Mack, L. Luer, D. Oelkrug, J. Chem. Phys. **116**, 8596 (2002)
37. A. Pogantsch, G. Heimel, E. Zojer, J. Chem. Phys. **117**, 5921 (2002)
38. Y. Han, S.U. Lee, J. Chem. Phys. **121**, 609 (2004)
39. A. Shukla, H. Ghosh, S. Mazumdar, Phys. Rev. B **67**, 245203 (2003)
40. S. Karabunarliev, M. Baumgarten, K. Mullen, J. Phys. Chem. A **104**, 8236 (2000)
41. H. Nakatsuji, J. Am. Chem. Soc. **95**, 345 (1973)
42. H. Nakatsuji, T. Koga, *The Force Concept in Chemistry* (Van Nostrand Reinhold, New York, 1981)
43. M. Belletete, S. Beaupre, J. Bouchard, P. Blandin, M. Leclerc, G. Durocher, J. Phys. Chem. B **104**, 9118 (2000)
44. M. Belletete, M. Bedard, M. Leclerc, G. Durocher, J. Mol. Struct.: THEOCHEM **679**, 9 (2004)
45. V. Lukes, D. Wegh, P. Hrdlovic, M. Stefko, K. Matsuzna, V. Laurinc, Syn. Met. **148**, 179 (2005)
46. A. Ojida, I. Hamachi, Bull. Chem. Soc. Jpn. **79**, 35 (2006)
47. A. Ojida, Y. Miyahara, J. Wongkongkatep, S. Tamaru, K. Sada, I. Hamachi, Chem. Asian J. **1**, 555 (2006)